RSC Advances

PAPER

View Article Online
View Journal | View Issue

Cite this: *RSC Adv.*, 2018, **8**, 38935

Efficient visible-light full-color tuning of self-organized helical superstructures enabled by fluorinated chiral switches†

Lang Qin, Wei Gu, Yingying Chen, Jia Wei* and Yanlei Yu

Received 14th September 2018
Accepted 13th November 2018

DOI: 10.1039/c8ra07657j

rsc.li/rsc-advances

Light-driven chiral switches have the ability to tune and control the self-organized helical superstructures of cholesteric liquid crystals (CLCs), resulting in the photo-induced reflection wavelength shift of the CLCs. A new type of axially chiral switch functionalized with fluorine atoms *ortho* to the azobenzene moiety is found to exhibit reversible visible-light-driven photoisomerization due to a separation of the n–π* absorption bands of the *trans* and *cis* isomers. These chiral switches all have high HTP values and the doped CLCs with 15.8 wt% concentration demonstrates reversible dynamic tuning of the reflection color within the entire visible spectrum driven by 530 nm and 445 nm visible light. It is also noteworthy that the thermal stability is improved thanks to the *cis* form of the fluorinated azobenzenes possessing a remarkably long half-life. The newly designed visible-light-driven chiral switches may broaden the application of CLCs, especially in the fields where high energy UV light is unfavorable.

Introduction

Cholesteric liquid crystals (CLCs) possessing self-organized helical superstructures[1] are a class of materials capable of selectively reflecting light according to Bragg's law. Dynamic tuning of reflection wavelength of the CLCs by external stimuli, including heat,[2,3] electric field,[4,5] chemical reaction[6,7] and light[8–16] is of great significance in many applications, such as color filters,[17] reflectors,[18,19] displays,[20,21] lasers,[22,23] and sensors.[24,25] Among all the stimuli, light wields advantages of remote, spatial and temporary controllability, therefore light-driven CLCs are widely studied.[26,27]

The commonly used method to obtain light-driven CLCs is to dope a small amount of photoresponsive chiral switches into nematic liquid crystals (LCs).[28,29] The ability of a chiral switch to twist the nematic LC into helical superstructures is represented by the helical twisting power (HTP, β) in the equation: $\beta = 1/(pc)$, where c is the concentration of the chiral switch and p is the pitch length of the helical superstructures. The central wavelength of the reflection λ is related to the pitch, *i.e.* defined as $\lambda = np$, where n is the average refraction index of the LC host. The configurational change of the chiral switches upon light irradiation enables the HTP variation, resulting in the photocontrol of the helices as well as the reflection wavelength.

Azobenzene-based chiral switches draw tremendous attention because of the dramatic difference in molecular geometry between the rod-like *trans* form and bent *cis* form, leading to large variation in HTP upon photoisomerization.[26] However, the necessity of high energy UV light to induce the *trans–cis* isomerization of normal azobenzene[30,31] impedes their practical applications, since UV light irradiation might bring about material decomposition and damage to biosamples. In this regard, developing photoresponsive CLCs that primarily respond to visible light and near-infrared (NIR) is highly desired for the wide utilizations.[12,13]

Li *et al.* developed NIR-light-tunable CLCs loaded with azobenzene-based chiral switches and upconversion nanoparticles (UCNPs). The UCNPs successfully converted NIR light of different power density to UV light or visible light, which triggered the *trans–cis* and *cis–trans* isomerization of the chiral switches respectively and realized the reversible tuning of the reflection wavelength in visible spectrum.[13] However, energy transfer from the UCNPs to the chiral switches resulted in low photoisomerization efficiency and slow response in this system. It is more straightforward to design novel chiral switches, whose photoisomerization in two directions can be induced by visible light. Recently, Li *et al.* designed and synthesized a special kind of azobenzene-based chiral switches possessing long conjugated structure. The reversible tuning of reflection colors from the doped CLCs was achieved by visible-light-driven photoisomerization.[12]

It has been proved that azobenzenes with *ortho*-fluorine atoms have lower energy of the *n*-orbital of the *cis* isomer, giving rise to a separation of n–π* absorption bands of the *trans* and *cis* isomers.[32,33] Green and blue light can therefore be used to

Department of Materials Science, State Key Laboratory of Molecular Engineering of Polymers, Fudan University, 220 Handan Road, Shanghai 200433, China. E-mail: weijia@fudan.edu.cn

† Electronic supplementary information (ESI) available. See DOI: 10.1039/c8ra07657j

induce the *trans–cis* and *cis–trans* isomerization, respectively. This inspired us to design chiral switches based on fluoroazobenzene to realize visible-light tuning of helical superstructures of the CLC. One should emphasize that Katsonis *et al.* recently have synthesized fluorinated chiral switches, but they have not reported the visible-light-driven photoisomerization and still used UV light to trigger the *trans–cis* process.[34] Herein, we reported the synthesis of axially chiral binaphthyl azobenzenes containing fluorine atoms *ortho* to azo moieties, which were proved to exhibit reversible visible-light-driven photoisomerization both in organic solvent and LC media (Fig. 1a). Furthermore, the chiral switches all exhibited high HTP values and only a small amount of the chiral switches successfully induced the formation of the helical superstructures. The CLCs formed by doping the chiral switches into nematic LC E7 generated the full-color dynamical change of the reflection driven by visible light with different wavelengths.

Results and discussion

Synthesis and characterization

The visible-light-driven chiral switches were prepared in a facile synthesis route (Fig. 1a and Experimental section Fig. 6), in which the 1,1′-binaphthyl group provides axial chirality and fluoroazobenzene moiety offers the distinct optical properties. Besides, the introduction of two mesogenic rod-like biphenyl enhances the solubility in commercially available nematic LC hosts including E7 and 5CB. The chemical structures of chiral switches were identified by ^{1}H, ^{19}F and ^{13}C NMR spectroscopy.

Visible-light-driven photoisomerization

UV-vis spectra were recorded to make clear the changes of the absorption of the chiral switches before and after sequential visible light irradiation at 530 nm and 445 nm. A solution of **S-1-5** in chloroform was placed in dark to maximize the absorption at 342 nm which corresponds to the π–π* absorption band of *trans o*-fluorinated azobenzene. As shown in Fig. 1b, 530 nm light irradiation triggered *trans–cis* isomerization evidenced by the intensity decrease of π–π* absorption band. In the visible part of the spectra (420–490 nm), two isobestic points at 428 nm and 464 nm were found due to the separation of n–π* absorption bands of the two isomers (Fig. 1c). The n–π* absorption band of *cis* isomer (450 nm) appeared with a slight blue-shift compared to that of *trans* isomer (468 nm), which is different from the parent azobenzenes without the substitution of electron-withdrawing fluorine atoms. The solution of **S-1-5** in chloroform took about 140 s to reach photostationary state (PSS) upon 530 nm light irradiation, whereas its reverse process took about 190 s to reach PSS_{445} by 445 nm light irradiation (Fig. 1d). Similar phenomena were also found in the other two chiral switches (Fig. S1 and S2, ESI†). These results indicate that both the *trans–cis* and *cis–trans* isomerization of the newly designed chiral switches can be fully triggered by visible light in solvent.

Measurement of HTP

Encouraged by the reversible visible-light-driven photoisomerization of the chiral switches in organic solvent, we doped the chiral switches into the commercially available nematic LC host to evaluate their HTP variation upon visible light irradiation. As shown in Fig. 2a and S3, ESI†, a small amount of the chiral switches (0.4 wt% in E7) successfully induced the formation of CLC phase, which was testified by the characteristic fingerprint textures observed by polarized optical microscope (POM), indicating that the chiral switches all have high HTP. The screw senses of the CLCs doped with the chiral switches were all determined to be left-handed according to the miscibility tests (Fig. S4, ESI†). The HTP values of the chiral

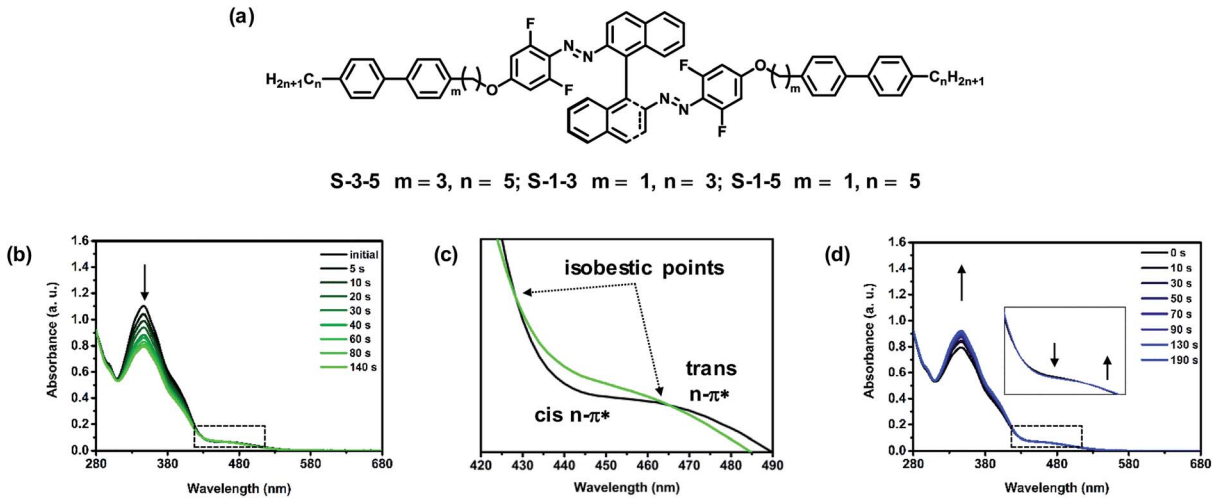

Fig. 1 (a) Chemical structure of the chiral switches studied in the experiment. (b) Changes of UV-vis absorption spectra of **S-1-5** in chloroform (2×10^{-5} M) upon irradiation of 530 nm light (27 mW cm^{-2}) from the initial state to the PSS_{530}. (c) Partial UV-vis absorption spectra of **S-1-5** between 420-490 nm showing the separation of n–π* bands of *trans* and *cis* isomers. (d) Changes of UV-vis absorption spectra of **S-1-5** in chloroform (2×10^{-5} M) upon irradiation of 445 nm light (0.4 mW cm^{-2}) from the PSS_{530} to the PSS_{445}.

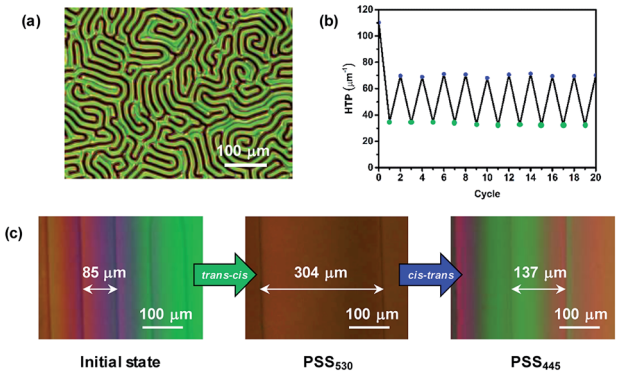

Fig. 2 (a) Fingerprint textures of 0.4 wt% **S-1-5** in E7 observed through POM. Scale bar, 100 μm. (b) Cycles of the changes of HTP of 1.0 wt% **S-1-5** in E7 upon alternate irradiation with 530 nm and 445 nm light. (c) POM images showing the distance changes of disclination lines of 1.0 wt% **S-1-5** in achiral LC E7 in the wedge cell before (left) and after sequential visible light irradiation at 530 nm (middle) and 445 nm (right).

switches were measured according to Grandjean–Cano method[35] (Fig. S5, ESI†). Taking the mixture of 1.0 wt% **S-1-5** in E7 as an example (Fig. 2c), the distance between disclination lines gradually increased from 85 to 304 μm and finally became stable at PSS_{530} thanks to the *trans–cis* isomerization of **S-1-5**. The resultant percent change in β was calculated as 72.4%. Reverse process occurred when irradiated with 445 nm light. The excellent fatigue resistance was confirmed by repeated irradiation of 530 nm and 445 nm light after many cycles and no obvious degradation was observed (Fig. 2b and S8, ESI†). Therefore, the reversible tuning of **S-1-5** was achieved only by visible light irradiation in LC media, which successfully induced the change of the helical superstructures. **S-3-5** and **S-1-5** also showed similar properties in CLC manipulation (Fig. S6–8, ESI†).

The HTP values of three chiral switches are summarized in Table 1. Compared to the previously reported visible-light-driven chiral switches,[12] these chiral switches all have higher HTP value at the initial state and more significant change of HTP upon light irradiation. The HTPs of **S-3-5** and **S-1-5** in 5CB are higher than that in E7, while **S-1-3** shows higher HTP value in E7 than in 5CB. The higher HTP of **S-3-5** and **S-1-5** in 5CB may arise from the higher degree of similarity between the end groups of chiral switches and 5CB host. Different LC hosts result in different intermolecular association between the chiral switches and the host. Therefore, we could conclude that subtle dependence of HTP exists on the molecular structures of both the dopant and the nematic LC host, which is consistent with previously reported results.[29] Moreover, HTP values of these chiral switches exhibit remarkable differences among various PSSs induced by visible light, which indicates reversible visible-light-tunable property of the chiral switches.

Table 1 Helical twisting power β (μm^{-1}, mol%) of the chiral switches in different nematic LC hosts at different states

		β (μm^{-1}, mol%)				
Sample	Host	Initial	PSS_{530}	PSS_{445}	$\Delta\beta^a$	$\Delta\beta/\beta_{ini}{}^b$ (%)
S-3-5	E7	100	28	59	72	72.4
	5CB	133	34	80	99	74.5
S-1-3	E7	152	39	78	113	74.5
	5CB	143	33	67	110	76.9
S-1-5	E7	110	32	69	78	70.6
	5CB	146	29	68	117	80.3

[a] Decrease. [b] Percent change in β from the initial state to the PSS_{530}.

Phototunable reflection

The high HTP value and the considerable difference among various states of the chiral switches allowed us to tune the reflection color of the CLC reversibly by visible light. Although **S-1-3** has higher HTP, the poor solubility in LC host (less than 10 wt%) indicates that it is not an ideal candidate for CLC manipulation. The HTP variation of **S-1-5** between PSS_{530} and PSS_{445} is larger than that of **S-3-5**. Therefore, **S-1-5** was chosen to demonstrate efficient tuning of the reflection color in CLC upon visible light irradiation. A mixture of 15.8 wt% **S-1-5** in achiral nematic LC E7 was filled into a 5 μm thick planar aligned cell *via* capillary force. Successfully, the CLC mixture exhibited reversible tuning of reflection color across the entire visible spectrum. At the initial state, the reflection band was located in the UV region (<400 nm). When irradiated with 530 nm light for 7 seconds, the cell appeared to be blue and the central reflection wavelength was shifted to around 440 nm. As shown in Fig. 3a and c, the reflection band red-shifted over the entire visible light region and the reflection color dynamically changed from blue *via* green to dark red upon continual 530 nm light irradiation within 27 s. The reverse process happened upon 445 nm light irradiation (Fig. 3b and d). Fig. 4 shows the real cell images of the CLC mixture in primary blue, green, red (RGB) reflection colors tuned by 530 nm and 445 nm light. Interestingly, a green and red "CLC" pattern in blue background was created by photomask technology. Therefore, reversible tuning of the reflection color and erasable patterning process of the CLC mixture were achieved in the visible spectrum, which is of significance in the practical display applications. These rewritable materials are expected to replace paper and lay the foundation for the realization of inkless printing technology. Besides, the reflection wavelength of the cell can be extended to NIR region (1175 nm) under irradiation of 530 nm light as expected. In the previously reported visible-light-driven CLC, high doping concentration of 22.7 wt% was needed to induce helical superstructures exhibiting dynamic reflection colors, which may narrow the temperature range of LC phase and increase viscosity of the CLC.[36] Here, the new types of visible-light-driven chiral switches possess high HTP value, which can efficiently induce and tune helical superstructures with low doping concentration.

Thermal relaxation

As is well-known, the application of light-directed RGB reflection colors change in CLCs doped with azo-based chiral

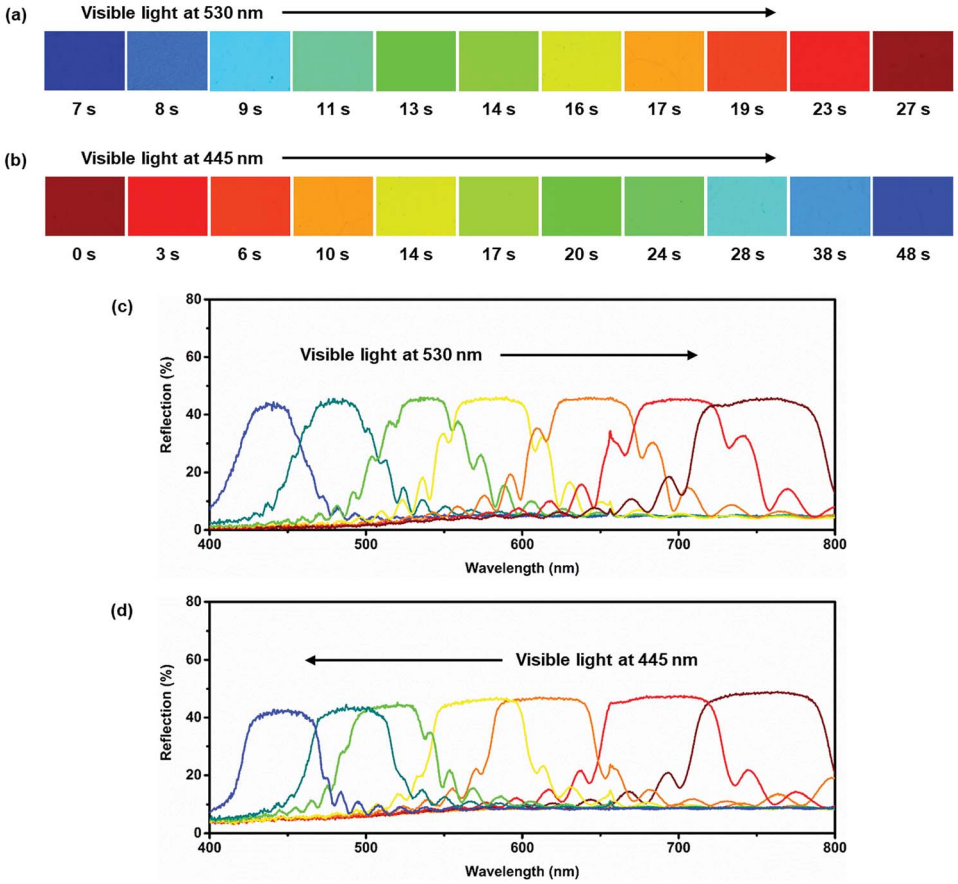

Fig. 3 Reflection color images of the CLC mixture in a 5 μm planar cell with 15.8 wt% **S-1-5** in E7 (a) upon consecutive visible light irradiation at 530 nm (15 mW cm^{-2}) and (b) 445 nm (0.4 mW cm^{-2}). Reflective spectra of the CLC mixture doped with 15.8 wt% **S-1-5** in E7 upon consecutive visible light irradiation at (c) 530 nm (15 mW cm^{-2}) and (d) 445 nm (0.4 mW cm^{-2}).

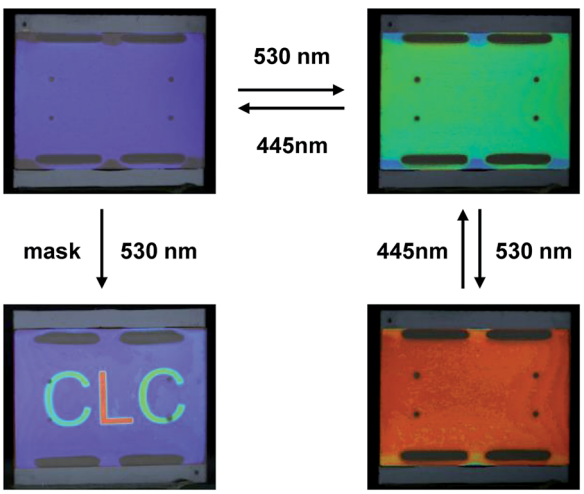

Fig. 4 Real cell images of CLC mixture in a 5 μm planar cell (2.0 cm × 2.5 cm) with 15.8 wt% **S-1-5** in E7 upon irradiation of visible light showing primary RGB colors and "CLC" pattern.

switches was limited because of the competing thermal back relaxation (*cis–trans* isomerization in darkness), which results in the lack of stability.[11] It's worth noting here that the thermal relaxation process of the reflection wavelength took about 50 hours through the entire visible region (Fig. 5), illustrating that our CLCs exhibit excellent thermal stability compared to that with common azo-based chiral switches without fluorine atoms, which is 10 hours.[37] The substitution of electron-withdrawing fluorine atoms may stabilize the *cis* isomers of the chiral switches and therefore lead to the excellent thermal stability of the CLCs.[29,34] Better thermal stability of our newly designed chiral switches results in color stabilities of the reflecting displays, which is of great importance in practical applications.

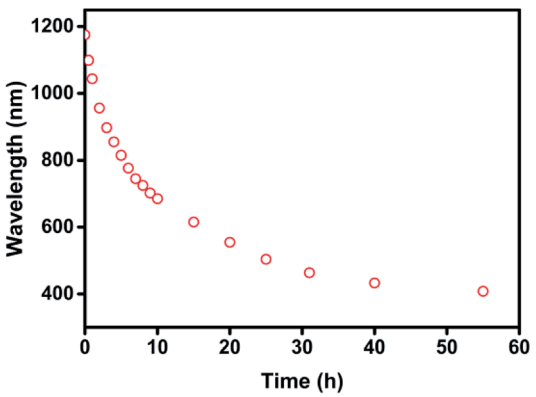

Fig. 5 Thermal back process of central reflection wavelength of 15.8 wt% **S-1-5** in E7 from the PSS_{530} at room temperature (25 °C).

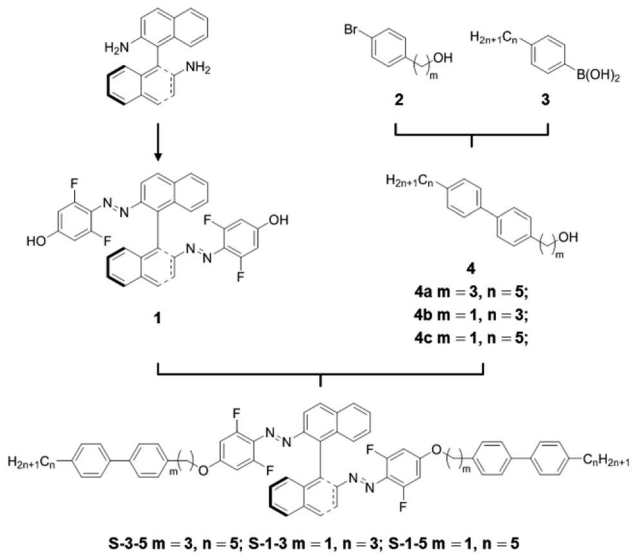

Fig. 6 Synthesis of visible-light-driven chiral switches.

Conclusions

In conclusion, we have designed a series of visible-light-driven chiral switches based on *o*-fluorinated azobenzene. The substitution of four fluorine atoms endows chiral switches with visible-light-driven two-way photoisomerization, and makes *cis* isomers more thermally stable at the same time. A small amount of **S-1-5** is able to efficiently induce self-organized helical superstructures in the CLC, whose reflection color is capable of being reversibly tuned in full-range visible spectrum. The investigation of these intriguing materials would assist full exploration of different potential applications of the CLCs, in which high energy UV light is unfavourable.

Experimental

Materials and methods

All chemicals and solvents were purchased from commercial suppliers and used without further purification. ^{1}H NMR, ^{13}C NMR and ^{19}F NMR spectra were recorded in $CDCl_3$. Chemical shifts are in δ units (ppm) with the residual solvent peak as the internal standard. The coupling constant (J) is reported in hertz (Hz). NMR splitting patterns are designed as follows: s, singlet; d, doublet; t, triplet; and m, multiplet. UV-vis spectrum was taken by a Perkin Elmer Lambda 650 Spectrometer. Textures, contact areas, reflection colors and distance changes of disclination lines were observed by a Leika DM2500p polarizing optical microscopy (POM). 530 nm light irradiation was carried out by a CCS HLV-24GR-3W LED light source. 445 nm light irradiation was carried out by a JD BL-445-300 laser light source. Reflection spectra of CLCs were examined with an Ideaoptica spectrometer.

Synthesis of chiral switches

Synthesis of intermediate 1. (*S*)-(−)-1,1′-Binaphthyl-2,2′-diamine (0.48 g, 1.7 mmol) was dissolved in a solution of H_2O (9 mL) and concentrated HCl (1.3 mL). The solution was cooled to 0 °C with ice water bath. A solution of sodium nitrite (0.29 g, 4.2 mmol) in H_2O (10 mL) was added dropwise with stirring. The solution of 3,5-difluorophenol (0.50 g, 3.87 mmol) and NaOH (0.45 g, 11.3 mmol) in H_2O (15 mL) was dropped into the resulting brown yellow suspension. The suspension was acidified with aqueous HCl and filtered. The precipitate was washed with H_2O and dried to get the crude product, which was purified by chromatography on silica gel with dichloromethane/ethyl acetate (19 : 1) to give a red brown solid (0.25 g, 26%). ^{1}H NMR (500 MHz, $CDCl_3$) δ = 8.19–8.05 (m, 4H), 7.98 (d, J = 8.2 Hz, 2H), 7.51 (t, J = 7.2 Hz, 2H), 7.34–7.21 (m, 4H), 6.17 (d, J = 12.8 Hz, 4H).

General procedure for the synthesis of intermediate 4. To a magnetically stirred mixture of **2** (1.0 mmol) and **3** (1.4 mmol) in toluene (20 mL) at ambient temperature under Ar atmosphere was added a solution of potassium carbonate (4.0 mmol) in H_2O (10 mL). A small amount of methyltrioctylammonium chloride and $Pd(PPh_3)_4$ were added to the solution. The reaction mixture was then slowly heated to reflux for 12 h and cooled to ambient temperature. The solvents were removed under reduced pressure. The crude product was purified by chromatography on silica gel with dichloromethane to give the white pure product.

4a. White solid, 89% yield. ^{1}H NMR (400 MHz, $CDCl_3$) δ = 7.50 (dd, J = 8.2, 6.6 Hz, 4H), 7.25 (t, J = 8.2 Hz, 4H), 3.71 (t, J = 6.4 Hz, 2H), 2.75 (t, J = 7.8 Hz, 2H), 2.63 (t, J = 7.8 Hz, 2H), 1.98–1.89 (m, 2H), 1.70–1.60 (m, 2H), 1.42–1.31 (m, 2H), 0.90 (t, J = 7.0 Hz, 3H). ^{13}C NMR (126 MHz, $CDCl_3$) δ = 141.89, 140.57, 138.84, 138.35, 128.80, 126.99, 126.82, 62.34, 35.59, 34.23, 31.72, 31.59, 31.21, 22.59, 14.07.

4b. White solid, 90% yield. ^{1}H NMR (500 MHz, $CDCl_3$) δ = 7.58 (d, J = 8.2 Hz, 2H), 7.51 (d, J = 8.2 Hz, 2H), 7.42 (d, J = 8.0 Hz, 2H), 7.25 (d, J = 8.1 Hz, 2H), 4.73 (s, 2H), 2.63 (t, J = 7.8 Hz, 2H), 1.72–1.66 (m, 2H), 0.98 (t, J = 7.3 Hz, 3H). ^{13}C NMR (500 MHz, $CDCl_3$) δ = 141.97, 140.65, 139.55, 138.16, 127.46, 127.17, 126.91, 65.19, 37.71, 24.58, 13.91.

4c. White solid, 96% yield. ^{1}H NMR (500 MHz, $CDCl_3$) δ = 7.59 (d, J = 8.2 Hz, 2H), 7.51 (d, J = 8.1 Hz, 2H), 7.43 (d, J = 8.4 Hz, 2H), 7.26 (d, J = 8.0 Hz, 2H), 4.74 (s, 2H), 2.64 (t, J = 7.8 Hz, 2H), 1.69–1.62 (m, 2H), 1.39–1.33 (m, 4H), 0.90 (t, J = 6.8 Hz, 3H). ^{13}C NMR (500 MHz, $CDCl_3$) δ = 142.20, 140.62, 139.57, 138.12, 128.84, 127.43, 127.13, 126.90, 65.14, 35.59, 31.57, 31.16, 22.56, 14.03.

General procedure for the synthesis of S-m-n. To a magnetically stirred solution 1 (1.0 mmol) and PPh_3 (3.0 mmol) in anhydrous THF (20 mL) at ambient temperature under Ar atmosphere was added dropwise a mixture of 4 (2.5 mmol) and diethyl azodicarboxylate (3.0 mmol) in THF (10 mL). The reaction mixture was then slowly warmed to reflux for 12 h and cooled to ambient temperature. The solvents were removed under reduced pressure. The crude product was purified by chromatography on silica gel with dichloromethane/petroleum ether (2 : 3) to give the orange product.

S-3-5. Orange solid, 60% yield. ^{1}H NMR (400 MHz, $CDCl_3$) δ = 8.11 (d, J = 9.0 Hz, 2H), 8.04–7.91 (m, 4H), 7.56–7.40 (m, 12H), 7.31–7.17 (m, 10H), 6.31 (d, J = 10.6 Hz, 4H), 3.86 (t, J = 6.3 Hz,

2H), 2.76 (t, J = 7.5 Hz, 4H), 2.67–2.58 (m, 4H), 2.10–2.01 (m, 4H), 1.69–1.60 (m, 4H), 1.39–1.31 (m, 8H), 0.91 (t, J = 6.8 Hz, 6H). ^{13}C NMR (126 MHz, $CDCl_3$) δ = 160.38, 158.28, 158.22, 156.20, 156.15, 149.57, 141.93, 139.63, 139.06, 138.24, 137.89, 134.63, 134.20, 128.87, 128.78, 128.03, 127.97, 127.18, 127.04, 126.80, 126.50, 113.56, 99.05, 98.84, 67.65, 35.58, 31.57, 31.50, 31.16, 30.29, 22.56, 14.03. ^{19}F NMR (400 MHz, $CDCl_3$) δ = −118.05. Mp: 63 °C; MS (ESI): $(M + H)^+$ 1095.51, found 1095.51.

S-1-3. Orange solid, 55% yield. ^{1}H NMR (500 MHz, $CDCl_3$) δ = 8.11 (d, J = 9.0 Hz, 2H), 7.98 (dd, J = 25.8, 8.5 Hz, 4H), 7.57 (d, J = 8.3 Hz, 4H), 7.53–7.35 (m, 12H), 7.31–7.23 (m, 6H), 6.41 (d, J = 10.4 Hz, 4H), 4.98 (s, 4H), 2.62 (t, J = 7.6 Hz, 4H), 1.73–1.62 (m, 4H), 0.97 (t, J = 7.3 Hz, 6H). ^{19}F NMR (400 MHz, $CDCl_3$) δ = −117.87. Mp: 85 °C; MS (ESI): $(M + H)^+$ 983.39, found 983.39.

S-1-5. Orange soild, 60% yield. ^{1}H NMR (400 MHz, $CDCl_3$) δ = 8.11 (d, J = 9.0 Hz, 2H), 8.04–7.90 (m, 4H), 7.56 (d, J = 8.2 Hz, 4H), 7.53–7.41 (m, 8H), 7.37 (d, J = 8.3 Hz, 4H), 7.31–7.21 (m, 6H), 6.40 (d, J = 10.4 Hz, 4H), 4.98 (s, 4H), 2.63 (t, J = 15.6 Hz, 4H), 1.65 (m, 4H), 1.38–1.32 (m, 8H), 0.90 (t, J = 14.0 Hz, 6H). ^{13}C NMR (126 MHz, $CDCl_3$) δ = 160.01, 158.23, 158.17, 156.15, 156.09, 149.58, 142.40, 141.40, 137.95, 137.85, 134.66, 134.17, 134.03, 128.90, 128.86, 128.05, 127.97, 127.89, 127.28, 127.23, 126.94, 126.53, 113.55, 99.49, 99.28, 70.47, 35.58, 31.55, 31.14, 22.55, 14.02. ^{19}F NMR (400 MHz, $CDCl_3$) δ = −117.86. Mp: 72 °C; MS (ESI): $(M + H)^+$ 1039.45, found 1039.45.

Conflicts of interest

There are no conflicts to declare.

Acknowledgements

This work is financially supported by the National Natural Science Foundation of China (51573029, 21734003), National Key R&D Program of China (2017YFA0701302), Natural Science Foundation of Shanghai (No.17ZR1440100) and Innovation Program of Shanghai Municipal Education Commission (Grant No. 2017-01-07-00-07-E00027).

Notes and references

1 H. K. Bisoyi and Q. Li, *Angew. Chem., Int. Ed.*, 2016, **55**, 2994.
2 D. J. D. Davies, A. R. Vaccaro, S. M. Morris, N. Herzer, A. P. H. J. Schenning and C. W. M Bastiaansen, *Adv. Funct. Mater.*, 2013, **23**, 2723.
3 K. Masuki, A. Takuya, S. Natsuki and W. Tatsuo, *Chem. Mater.*, 2009, **21**, 564.
4 J. Xiang, Y. N. Li, Q. Li, D. A. Paterson, J. M. D. Storey, C. T. Imrie and O. D. Lavrentovich, *Adv. Mater.*, 2015, **27**, 3014.
5 C. A. Bailey, V. P. Tondiglia, L. V. Natarajan, M. M. Duning, R. L. Bricker, R. L. Sutherland, T. J. White, M. F. Durstock and T. J. Bunning, *J. Appl. Phys.*, 2010, **107**, 013105.
6 A. Saha, Y. Tanaka, Y. Han, C. M. W. Bastiaansen, D. J. Broer and R. P. Sijbesma, *Chem. Commun.*, 2012, **48**, 4579.
7 Y. Han, K. Pacheco, C. W. M. Bastiaansen, D. J. Broer and R. P. Sijbesma, *J. Am. Chem. Soc.*, 2010, **132**, 2961.
8 T. J. White, M. E. McConney and T. J. Bunning, *J. Mater. Chem.*, 2010, **20**, 9832.
9 Q. Li, Y. Li, J. Ma, D.-K. Yang, T. J. White and T. J. Bunning, *Adv. Mater.*, 2011, **23**, 5069.
10 M. Mathews and N. Tamaoki, *J. Am. Chem. Soc.*, 2008, **130**, 11409.
11 Y. Li, A. Urbas and Q. Li, *J. Am. Chem. Soc.*, 2012, **134**, 9573.
12 Y. Wang, A. Urbas and Q. Li, *J. Am. Chem. Soc.*, 2012, **134**, 3342.
13 L. Wang, H. Dong, Y. Li, C. Xue, L.-D. Sun, C.-H. Yan and Q. Li, *J. Am. Chem. Soc.*, 2014, **136**, 4480.
14 Y. Kim and N. Tamaoki, *J. Mater. Chem. C*, 2014, **2**, 9258.
15 S. Kurihara, S. Nomiyama and T. Nonaka, *Chem. Mater.*, 2001, **13**, 1992.
16 Q. Li, L. F. Li, J. Kim, H.-S. Park and J. Williams, *Chem. Mater.*, 2005, **17**, 6018.
17 J. Lub, P. van de Witte, C. Doornkamp, J. P. A. Vogels and R. T. Wegh, *Adv. Mater.*, 2003, **15**, 1420.
18 U. A. Hrozhyk, S. V. Serak, N. V. Tabiryan, T. J. White and T. J. Bunning, *Opt. Express*, 2010, **18**, 9651.
19 L. De Sio, T. Placido, S. Serak, R. Comparelli, M. Tamborra, N. Tabiryan, M. L. Curri, R. Bartolino, C. Umeton and T. Bunning, *Adv. Opt. Mater.*, 2013, **1**, 899.
20 T. Yoshioka, T. Ogata, T. Nonaka, M. Moritsugu, S.-N. Kim and S. Kurihara, *Adv. Mater.*, 2005, **17**, 1226.
21 E. Montbach, N. Venkataraman, A. Khan, I. Shiyanovskaya, T. Schneider, J. W. Doane, L. Green and Q. Li, *SID Int. Symp. Dig. Tech. Pap.*, 2008, **39**, 919.
22 S. M. Morris, P. J. W. Hands, S. Findeisen-Tandel, R. H. Cole, T. D. Wilkinson and H. J. Coles, *Opt. Express*, 2008, **16**, 18827.
23 S. Furumi and N. Tamaoki, *Adv. Mater.*, 2010, **22**, 886.
24 M. Moirangthem, R. Arts, M. Merkx and A. P. H. J. Schenning, *Adv. Funct. Mater.*, 2016, **26**, 1154.
25 D. J. Mulder, A. P. H. J. Schenning and C. W. M. Bastiaansen, *J. Mater. Chem. C*, 2014, **2**, 6695.
26 H. K. Bisoyi and Q. Li, *Chem. Rev.*, 2016, **116**, 15089.
27 J. Lu, W. Gu, J. Wei, W. Zhang, Z. Zhang, Y. Yu, N. Zhou and X. Zhu, *J. Mater. Chem. C*, 2016, **4**, 9576.
28 Y. Wang and Q. Li, *Adv. Mater.*, 2012, **24**, 1926.
29 H. K. Bisoyi and Q. Li, *Acc. Chem. Res.*, 2014, **47**, 3184.
30 T. J. White, R. L. Bricker, L. V. Natarajan, N. V. Tabiryan, L. Green, Q. Li and T. J. Bunning, *Adv. Funct. Mater.*, 2009, **19**, 3484.
31 Y. Xie, D. Fu, O. Jin, H. Zhang, J. Wei and J. Guo, *J. Mater. Chem. C*, 2013, **1**, 7346.
32 D. Bléger, J. Schwarz, A. M. Brouwer and S. Hecht, *J. Am. Chem. Soc.*, 2012, **134**, 20597.
33 L. Qin, W. Gu, J. Wei and Y. Yu, *Adv. Mater.*, 2018, **30**, 1704941.
34 H. Huang, T. Orlova, B. Matt and N. Katsonis, *Macromol. Rapid Commun.*, 2017, **39**, 1700387.
35 G. Heppke and F. Oestreicher, *Z. Naturforsch. A*, 1977, **32**, 899.
36 K. Akagi, *Chem. Rev.*, 2009, **109**, 5354.
37 J. Ma, Y. N. Li, T. White, A. Urbas and Q. Li, *Chem. Commun.*, 2010, **46**, 3463.

